Context specific ubiquitin modification of ribosomes regulates translation under oxidative stress

Shannon E. Dougherty[1], Géssica C. Barros[1], Matthew W. Foster[2] , Guoshou Teo[3], Hyungwon Choi[3], Gustavo M. Silva[1]

[1]Department of Biology, Duke University, Durham, NC 27708, USA
[2]Division of Pulmonary, Allergy and Critical Care, Department of Medicine, Duke University Medical Center, Durham, North Carolina.
[3]Department of Medicine, Yong Loo Lin School of Medicine, National University of Singapore, Singapore, Singapore

ABSTRACT:

Cellular exposure to oxidative stress is known to activate several translational control pathways through ribosome ubiquitination. Two such pathways, Redox-control of translation by ubiquitin (RTU) and Ribosome-associated quality control (RQC), modify the ribosome with K63-linked polyubiquitination, but result in two different ribosome fates. RTU responds to peroxide stress exposure by inducing a burst or ribosome polyubiquitination and subsequent pause of translational elongation. Alternatively, RQC leads to ubiquitination of already stalled ribosomes and mediates their clearance through subunit dissociation. Understanding how site-specific ribosome ubiquitination induces translation regulation is difficult due to the simultaneous occurrence of these distinct translational control pathways. Here we develop a targeted proteomics approach to quantify site-specific ubiquitin modification across the ribosome in steady state and stress conditions. We found several sites to be differentially ubiquitinated due to stress, including sites known to be targeted by the RQC. The results indicate that the RTU and RQC target distinct ribosome subpopulations within the cell, and differentially contribute to the cellular stress response in an oxidative stressor-specific manner. These findings significantly contribute to the dissection of the complex coordination of translation in response to stress and shed light on the integration of important quality control pathways during cellular response to stress.

INTRODUCTION

Cells adapt to stress in specific ways to ensure survival in ever-changing conditions. One way cells adapt is by instituting specific gene expression programs to combat stress (de Nadal *et al*, 2011; Gasch *et al*, 2000). While genomic and transcriptomic induction of stress-specific gene expression programs have been extensively investigated (Mascarenhas *et al*, 2008; Taymaz-Nikerel *et al*, 2016), many aspects of the induction at the proteomic level remain unclear. In response to many forms of stress, cells suppress global translation while simultaneously inducing the production of selective stress-response proteins (Barros *et al*, 2023; Shenton *et al*, 2006). This global suppression is crucial to prevent damage to newly synthesized proteins, prevent toxic gain-of-functions, and minimize extraneous energy expenditure on non-essential proteins (Holcik & Sonenberg, 2005). Some mechanisms, such as the Integrated stress response (ISR), are known to block the initiation stage of translation (Pakos-Zebrucka *et al*, 2016), but the regulation of ribosomes in the elongation step of translation has not been studied as extensively (Barros *et al.*, 2023; Shenton *et al.*, 2006). As regulation of elongating ribosomes is critical for rapid response to dynamic cellular conditions (Shenton *et al.*, 2006), understanding the mechanisms underlying this regulation is vital to comprehend how cells respond and adapt to stressful conditions.

The Redox-control of translation by ubiquitin pathway (RTU) is one pathway known to regulate elongation and support cell adaptation to stress in yeast (Dougherty *et al*, 2020; Silva *et al*, 2015). As its name suggests, the RTU pathway is activated by oxidative stress and employs ubiquitin to arrest ribosomes in the pre-translocation stage of elongation (Zhou *et al*, 2020). In response to hydrogen peroxide (hereafter H_2O_2 or peroxide) stress, the RTU E2 ubiquitin conjugase, Rad6, and E3 ubiquitin ligase, Bre1, heavily modify ribosomes with K63-linked polyubiquitin chains (Silva *et al.*, 2015; Simões *et al*, 2022). K63 polyubiquitin differs from the more common K48-linked polyubiquitin as it does not signal the target for proteasomal degradation (Manohar *et al*, 2019), but instead has been shown to serve as a regulatory signal in functions such as DNA repair, intercellular trafficking, and immune signaling pathways (Erpapazoglou *et al*, 2014; Liu *et al*, 2018; Madiraju *et al*, 2022). Recent findings suggest Rad6-mediated ubiquitination plays a role in mediating ribosome pausing on XIP motifs and contributes to mechanisms of translation repression, but the connection between ribosome ubiquitination and translation control remains unclear (Meydan *et al*, 2023).

In the RTU pathway, maximum accumulation of K63-linked ubiquitin was found to occur after 30 minutes of exposure to 0.6 mM H_2O_2 (Silva *et al.*, 2015). Under this H_2O_2 condition, our previous work identified the presence of 78 ub-modified ribosomal protein lysine residues following enrichment for K63 polyubiquitinated proteins by the K63-TUBE specific antibody (Back *et al*, 2019). As ub-modified site presence was determined in comparison to a K63R null control, which ub-modifications occur in a stress-responsive manner remains unclear. Further investigation into ub-modified sites has proven difficult due to the low abundance of ubiquitinated proteins to their non-ubiquitinated counterparts, the methodological limitations of investigating each site independently, and the existence of multiple ubiquitin-mediated processes of ribosome regulation (Dougherty *et al.*, 2020; Garshott *et al*, 2020; Inada, 2020).

One such complicating ubiquitin-mediated process is the Ribosome-associated protein quality control pathway (RQC) (Matsuo & Inada, 2023). In the RQC, stalled ribosomes are recognized and modified with K63-linked polyubiquitin chains by the ubiquitin ligase Hel2 (Matsuo

et al, 2017). This ubiquitin signal recruits factors to dissociate the stalled ribosome from the mRNA transcript and ultimately results in degradation of the nascent peptide by the proteasome (Matsuo *et al*, 2023). While previous work has established that the RTU ribosome ubiquitination occurs independently of Hel2 and suggests an alternative fate to that of ribosome dissociation (Silva *et al.*, 2015; Simões *et al.*, 2022; Zhou *et al.*, 2020), how the RTU and RQC pathways are coordinated remains unknown.

To dissect the dynamics of ribosome ubiquitination under stress, here we developed a new proteomics method, to detect and quantify site-specific ubiquitination across 79 ribosome sites as well as quantify the abundance of 4 ubiquitin linkage types. We utilized this proteomics method to characterize the ubiquitin-modified ribosome landscape and identified 11 ribosomal sites that were ubiquitinated in response to H_2O_2 stress, including 2 known targets of the RQC Then, using the known RQC-inducing oxidizing agent 4-nitroquinoline 1-oxide (4-NQO), we explored the dynamics of oxidative stress on ribosomal protein ubiquitination. and found the RTU and RQC are sensitive to distinct oxidative stressors and target different ribosome subpopulations. We confirmed that the RTU induces further translational control by inducing the Integrated stress response (ISR) in response to peroxide, but not 4-NQO stress. Finally, we showed the RQC pathway mitigates the ISR in response to low concentration of 4-NQO stress, but not in H_2O_2. Collectively our data suggests that different oxidizing stressors lead to distinct ribosome site ubiquitination, which results in distinct regulation of translation and induction of oxidizing stressor specific cell response mechanisms.

RESULTS

Characterization of the landscape of ub-modified ribosome sites in H_2O_2 stress

To understand the role of ubiquitin in regulating ribosome elongation as part of the RTU, we first sought to detail the landscape of ub-modified ribosome sites. To do so, we developed a two-step ubiquitinated ribosome enrichment protocol coupled with Parallel Reaction Monitoring Mass Spectrometry (PRM-MS) which we dubbed Ribosome-target Parallel Reaction Monitoring (Rt-PRM) (Ordureau *et al*, 2018). PRM is an ideal method to overcome the complications of investigating ub-modified sites due to its high sensitivity, selectivity, and throughput capabilities (Peterson *et al*, 2012). PRM reduces interference from non-targets through mass-to-charge (m/z) filtering and monitors all product ions, enabling the detection, identification, and quantification of low-abundance species such as those derived from ubiquitinated proteins. This filtering and parallel monitoring also allow the simultaneous detection and quantification of multiple coexisting targets. To apply PRM-MS to ubiquitinated ribosomes under stress, log phase yeast cells were collected before and after treatment with 0.6 mM H_2O_2 and lysed. Ribosomes were then isolated by sucrose sedimentation followed by tryptic digestion (Fig 1A). We designed a set of 103 heavy-labeled (C-terminal Lysine (13C6,15N2) or Arginine(13C6,15N4)) reference tryptic peptides containing a K-GG remnant for all ub-modified ribosome sites identified under stress in addition to all ubiquitin linkage types (Table S1) (Back *et al.*, 2019). The heavy-labeled peptides served as both a guide for PRM mass-to-charge (m/z) filtering and an internal control for biological peptide quantification. The samples were then spiked with the heavy-labeled reference peptides prior to the enrichment of ubiquitinated protein-derived peptides using a K-GG remnant-specific antibody.

Ub-modified peptides enriched by this two-step enrichment protocol were then analyzed by LC-MS/MS in a process we dubbed Rt-PRM. Of the 103 designed heavy labeled peptides, 82 were successfully detected via data-dependent acquisition (DDA) mass spectrometry analysis and were employed to guide PRM m/z filtering for targeting of the biologically derived peptides (Table S2). K-GG peptides were then identified and quantified using a combination of Skyline proteomics (MacLean *et al*, 2010) and the developed PRMKit software (Fig S1A).

To assess the validity of Rt-PRM in capturing the H_2O_2-induced accumulation of K63-linked polyubiquitin detected via western blot (Fig 1B) (Silva *et al.*, 2015), we compared the abundance of K63-linked signature ubiquitin peptide (Ub.K63) detected in H_2O_2 treated and untreated conditions (Fig 1C). Our proteomics analysis revealed that the abundance of K63.Ub increased more than 4-fold in treated conditions. Measurement of other ubiquitin linkage signature peptides revealed that K48-linked ubiquitin (Ub.K48) also increased in response to peroxide treatment, while Ub.K11 showed no significant increase (Fig 1C). These findings align with published trends for lysine-specific ubiquitin linkage type increases in peroxide stress (Manohar *et al.*, 2019; Silva *et al.*, 2015).

Of the 82 K-GG quantified peptides, 17 peptides, including Ub.K63, Ub.K48, and 13 ribosome ubiquitin sites, showed a statistically significant increase in H_2O_2 treatment compared to untreated conditions (Fig 1D). Of these significant ub-modified sites, 11 underwent a greater than 2x fold-change in K-GG peptide in H_2O_2 treatment, with two sites, uS10.K8 and uS8.K88 increasing more than 4-fold (Fig 1E). Our method also allowed us to quantify the absolute abundance of peptides through normalization of biological peptide intensity values by the intensity of the site-specific spiked heavy reference peptide. We observed that 9 of the more than 2-fold increasing ub-modified sites occurred in the range of 0.1-1 fmol per mg of isolated ribosome (Fig 1E. S1B). 2 of the 11 sites, uS10.K8 and uS5.K33, were found to occur at more than 50 fmol per mg of ribosome (Fig 1E). These 2 ub-modified sites are both located on the beak of the 40S ribosomal subunit, a region well-established as a hub for translational regulation (Fig 1F) (PDB 6XIR) (Llácer *et al*, 2015; Meng *et al*, 2023; Wilson & Doudna Cate, 2012; Zhou *et al.*, 2020). Interestingly, uS10.K8 and uS5.K33 are also reported as target sites for ub-modification by the Ribosome-associated protein quality control pathway (RQC) (Garshott *et al.*, 2020; Matsuo *et al.*, 2017; Yan *et al*, 2019), raising questions as to whether Hel2 is responsible for the site-specific ub-modification observed in our proteomics analysis.

As previously established (Silva *et al.*, 2015; Simões *et al.*, 2022), the accumulation of K63-linked ubiquitin in peroxide stress occurs even in *HEL2* deleted cells (Fig 2A), suggesting Hel2 is not the main mediator of this K63 under H_2O_2. The Hel2-independence of ubiquitin accumulation in H_2O_2 was confirmed by label-free mass spectrometry of enriched K-GG containing peptides from ribosome isolates, as Ub.K63, Ub.K48, and Ub.K11 peptides showed similar H_2O_2-induced increases in *hel2Δ* cells (Fig 2B), as was seen for wild-type (WT) in Figure 1C. However, measurement of fold-change of uS10.K8 and uS5.K33 ubiquitination in H_2O_2-treated to untreated cells revealed a decreased stress-induced ubiquitination in the *hel2Δ* derived peptides (Fig 2C), as compared to WT in Figure 1E. When compared to the WT, we saw a 7-fold reduction of H_2O_2 induced ub-modified uS5.K33 *hel2Δ* (Fig 2C). This observation suggests that ub-modification of uS5.K33 is dependent on Hel2 (Garshott *et al.*, 2020; Yan *et al.*, 2019). While the K-GG containing uS10.K8 peptide showed a more than 5-fold decrease of H_2O_2 ub-modification in *hel2Δ* compared to WT (Fig 2C), quantification of fold-change due to H_2O_2

treatment within *hel2Δ* still showed a more than 2-fold increase compared to untreated levels. This data suggests that while the increase in ub-modified uS10.K8 in H_2O_2 is regulated by Hel2 (Matsuo *et al.*, 2017), there may be some H_2O_2 induced uS10.K8 ubiquitination independent of Hel2. Further investigation of the ub-modified sites in *hel2Δ* revealed four sites, uL5.K35, eS25.K52, eL22.K99, and uL5.K49, that significantly increased from untreated to H_2O_2-treated conditions regardless of Hel2 expression (Fig 2D). While eL22.K99 is located on the large ribosomal subunit far from the decoding center, uL5.K35, eS25.K52, and uL5.K49 are adjacent to the tRNA-binding E site, and thus site modification could interfere with translational elongation (Fig 2E) (Wilson & Doudna Cate, 2012). Furthermore, this analysis suggested that the increase of ubiquitinated uS5.K33 and uS10.K8 in H_2O_2 stress is Hel2-dependent, suggesting that RQC activity is induced by H_2O_2 stress. As the burst of K63 ubiquitin in H_2O_2 occurs independently of Hel2, our proteomics findings raise questions as to how peroxide induction of the RQC mechanism is coordinated with induction of the RTU response.

Sensitivity of the RQC and RTU pathways to distinct stressors

Our proteomic analysis of the ub-modified ribosome landscape suggests that the RTU and RQC may be simultaneously induced in response to oxidative stress. It has been previously shown that RQC ribosome ubiquitination occurs across several specific ribosome sites in yeast, including uS10.K6/8, uS5.K33, and uS3.K212 in a Hel2-dependent manner (Garshott *et al.*, 2020; Higgins *et al*, 2015; Matsuo *et al.*, 2017; Sugiyama *et al*, 2019). Recent work has revealed an increased the previously highlighted RQC ub-modified sites in response to 4-nitroquinoline 1-oxide (4-NQO), a nucleotide-targeting oxidizing agent (Yan *et al.*, 2019), but whether this increased RQC site-specific ub-modification is also induced by H_2O_2 stress has not been studied. Additionally, the RTU redox burst of K63 polyubiquitin has been observed under H_2O_2 stress but not due to non-peroxide stressors (Silva *et al.*, 2015). However, whether 4-NQO induces this K63 ubiquitin burst has not been directly investigated.

To determine if the RTU and RQC pathways are simultaneously induced in oxidative stress, we first questioned whether the redox-induced burst of K63 polyubiquitin occurred in both H_2O_2 and 4-NQO stress (Figure 3C). We found that K63 polyubiquitin accumulated in the lower concentration of H_2O_2 stress (0.6 mM) but not in 5 mM H_2O_2 or 4-NQO. Furthermore, we found that the deletion of *HEL2* did not alter the H_2O_2 specificity of K63 polyubiquitin accumulation. Deletion of *RAD6*, however, did prevent K63 Ub accumulation in H_2O_2 stress. This data confirms previous findings on the peroxide-specific induction of the RTU (Silva *et al.*, 2015), and suggests that if simultaneous induction of the RTU and RQC does occur, it would be a distinct mechanism to peroxide stress.

Previous work found exposure to 4-NQO or the alkylating agent methyl methanesulfonate (MMS) damaged mRNA, activating the no-go-decay pathway (NGD), an RQC-associated mRNA surveillance mechanism (Yan *et al.*, 2019). Like the RQC, NGD-targeted degradation of mRNA is dependent on the E3 Hel2, and its induction can be measured through the Hel2-dependent ubiquitination of the small ribosomal protein uS3 at lysine 212 (Matsuo *et al.*, 2017; Sugiyama *et al.*, 2019). To determine whether the RQC is activated similarly across multiple types of oxidative stress, we sought to compare the dynamics of RQC-mediated ribosome site-specific ubiquitination in H_2O_2 stress to those observed in response to treatment with 4-NQO (Yan *et al.*,

2019). We first measured the levels of ubiquitinated uS3 under H_2O_2 and 4-NQO stress (Fig 3B). Treatment with the mRNA alkylating agent MMS was used as a control for ROS-independent induction of NGD and uS3 ubiquitination (Yan *et al.*, 2019). Monoubiquitinated uS3 (uS3-Ub_1) was detected in 4-NQO and MMS stress but under H_2O_2, suggesting peroxide does not induce NGD. Upon *HEL2* deletion, we detected a loss of uS3-Ub_1 in MMS stress but not in 4-NQO. The presence of some mono-ubiquitinated uS3 in 4-NQO in *hel2Δ* is contrary to expectations of Hel2-dependence of NGD (Matsuo *et al.*, 2017; Sugiyama *et al.*, 2019). To control for the potential effects of cross-talk between the RTU and RQC, we also measured stress-induced uS3 ubiquitination in *rad6Δ* (Fig 3B) but found no difference from WT. In all, these findings demonstrate that if the RQC is induced by H_2O_2, it is unlikely to be through the same mechanisms of induction by 4-NQO or MMS stress.

Finally, the previous work into stress-induction of the RQC found that in addition to inducing NGD, exposure to 4-NQO also increased site-specific ubiquitination of uS5.K33 and uS10.K8 (Yan *et al.*, 2019). To determine whether H_2O_2 stress induced the ubiquitination of these sites, and therefore RQC, to the same extent as seen for 4-NQO stress, we measured the presence of ubiquitinated endogenously expressed 3HA-tagged uS5 or uS10. While we were not able to definitively identify the occurrence of polyubiquitinated uS5-3HA in any stress conditions (Fig S3A), we did detect polyubiquitinated forms of uS10-3HA in H_2O_2, 4-NQO, and MMS (Fig 3C). The presence of ubiquitinated uS10-3HA further validates our proteomics findings that H_2O_2 stress induces uS10 ubiquitination. Furthermore, the amount of ubiquitinated uS10-3HA species was similar between H_2O_2 and 4-NQO, suggesting that while H_2O_2 does not induce uS3 ubiquitination, it may induce the RQC through as yet unestablished mechanisms. Taken together with the 4-NQO and MMS-specific presence of monoubiquitinated uS3, these findings suggest that the RQC and RTU pathways may target and ubiquitinate distinct subpopulations of ribosomes within the cell.

As we were unable to confirm H_2O_2 induction of the RQC through the measurement of ubiquitinated RQC ribosomal sites, we questioned whether stress induction could be detected through the association of RQC ubiquitin-related proteins with the ribosome. To determine whether the RQC ubiquitin ligase, Hel2, was differentially recruited to ribosomes during stress, we measured the association of exogenous FLAG-tagged Hel2 with sucrose-sedimented ribosomes (Fig 3D, Fig S3B). We found that FLAG-tagged Hel2 association with ribosomes did not differ due to exposure to any stress. Although there was no evidence that stress alters Hel2 ribosome recruitment, we questioned whether stress might disrupt the recognition of ub-modified ribosomes by downstream RQC factors. The RQC factor, Cue3, contains a ubiquitin-binding domain and is important to recruit ribosome dissociating proteins to ubiquitinated stalled ribosomes (Matsuo *et al.*, 2023). To determine whether stress affected the recruitment of RQC dissociating factors, we examined the association of exogenous FLAG-tagged Cue3 with sucrose-sedimented ribosomes (Fig 3E, Fig S3C). Like the findings for Hel2-FLAG, Cue3-FLAG did not show differential association with isolated ribosomes in untreated or stress treated conditions. These findings suggest that if there are stress-specific effects on the recruitment of RQC factors to the ribosome, the interactions are too transient to capture via sucrose sedimentation.

We sought to determine whether the RQC is induced in a stress-specific manner by testing the ability of the RQC to clear stalled ribosomes using an established reporter system (Matsuo *et al.*, 2017). The inducible dual-luciferase reporter contains either a No-Stall control or 6xCGA

polyarginine sequence inserted between Renilla luciferase (Rluc) and Firefly (Fluc) encoding regions (Fig 4C) (Meydan *et al.*, 2023). Stretches of positively charged peptide sequences, especially those encoded by rare codons like CGA, are known to induce ribosome stalling (Barros *et al*, 2021; Chen *et al*, 2024; Matsuo *et al.*, 2017). As RQC-mediated clearance of stalled ribosomes culminates in nascent peptide degradation and translation abortion, the efficiency of RQC clearance of 6xCGA stalls can be quantified by reduction of the Fluc/Rluc ratio. In wild-type (WT) cells, the 6xCGA Fluc/Rluc ratio was 10-fold less than the No-Stall control (Fig 4A), confirming that the 6xCGA sequence stalled translation. In *hel2Δ* the Fluc/Rluc ratio was only 4-fold less than the No-Stall control. This data indicates that in the absence of the RQC pathway, ribosomes stalled on the 6xCGA sequence are not cleared by ribosome dissociation and instead are able to bypass the troublesome sequence to produce more Firefly luciferase.

If stress induces RQC activity, one expects more clearance of 6xCGA stalled ribosomes, as shown by a further reduction of the Fluc/Rluc ratio compared to the No-Stall control. Contrary to these expectations, we found no significant difference in wild-type (WT) Fluc/Rluc signal upon treatment with 4-NQO or H_2O_2 treatment. Both oxidative stress exposures also did not alter the Fluc/Rluc ratio of the 6xCGA reporter in *hel2Δ* compared to untreated conditions, suggesting that while there was no detectible pathway induction, the RQC is still able to clear 6xCGA stalled ribosomes in oxidative stress conditions. Additionally, RQC activity was unaffected by modulations of RTU pathway activity as deletion of *RAD6* had no significant effect on the Fluc/Rluc ratio in any condition (Fig S4A). If the RQC and RTU pathways were to compete for ribosome targets, we would anticipate an increase in RQC activity in the absence of Rad6. However, we did not observe upregulation of RQC activity in any condition in *rad6Δ*, thus lending support to the notion that RQC and RTU target distinct subpopulations of ribosomes within the cell. While the inducible dual-luciferase reporter is a valuable tool for detecting differences that may arise over a brief period of stress treatment, it is possible that the duration between expression induction and Fluc/Rluc signal detection was too brief for any noticeable differences to accumulate due to deletion of *RAD6*, potentially masking competition between the two pathways. Together these findings suggest that RQC-mediated clearance of the stall-inducing 6xCGA sequence is present but not further activated in a stress-specific manner.

To determine whether inhibition of the RTU through deletion of *RAD6* impacted the ability of the RQC to clear 6xCGA stalled ribosomes over a more extended period, we employed the use of an established GFP-FLAG-HIS3 reporter containing a 6xCGA sequence between the GFP and FLAG-HIS3 transcripts (Fig 5A) (Matsuo *et al.*, 2017). As this reporter is constitutively expressed, the effect of *RAD6* deletion on RQC clearance of 6xCGA stalled ribosomes can be measured over a prolonged period, although this also prevents the ability to use this construct to determine changes due brief stress exposure. As such, we measured the amount of 6xCGA translation bypass in WT, *hel2Δ*, and *rad6Δ* cells using GFP and FLAG antibodies to detect the amount of full-length protein via western blot in untreated conditions (Fig 5B). A No-Stall sequence insert served as a control for reporter expression differences due to strain background. While the expression of the full-length No-Stall construct was consistent across cell backgrounds, in WT, the 6xCGA construct was cleared by the RQC, resulting in less full-length protein expression. Upon RQC inhibition by deletion of *HEL2*, translation is able to bypass the 6xCGA sequence, and expression of some full-length protein is restored, thus reaffirming the 6xCGA sequence induces RQC-mediated clearance of stalled ribosomes and nascent peptide degradation (Matsuo *et al.*,

2017; Meydan *et al.*, 2023). In *rad6Δ*, we observed a slight decrease in the amount of full-length protein compared to WT upon probing with anti-FLAG. This *rad6Δ* decrease in 6xCGA bypass suggests that there is increased RQC clearance of 6xCGA stalled ribosomes in the absence of the RTU ubiquitin conjugase (Fig 5C).

To determine if the increased decreased 6xCGA bypass in *rad6Δ* mutant could be rescued, we measured the amount of full-length 6xCGA protein product in *rad6Δ* mutants expressing exogenous HA-tagged Rad6 or the catalytically dead Rad6^{C88S} mutants (Fig 5D) (Simões *et al.*, 2022). The expression of exogenous Rad6 was confirmed with the anti-Rad6 antibody, which revealed higher Rad6 than was expressed endogenously in WT. Expression of exogenous Rad6 not only restored the amount of full-length reporter protein expression to WT amounts but also appeared to exacerbate the bypass of the 6xCGA stalling sequence. These findings, combined with the increased amount of Rad6 from exogenous expression, suggest an inverse relationship between the amount of Rad6 and the ability of the RQC to clear ribosomes stalled by 6xCGA. As the 6xCGA bypass also increased upon expression of the Rad6^{C88S} mutant, this inverse relationship seems to depend on the level of Rad6 and not its activity as a ubiquitin conjugase. We also measured 6xCGA bypass in Rad6 mutants known to either increase or decrease ribosome association but found no correlation between Rad6 ribosome affinity and RQC-clearance of stalled ribosomes (Fig S5A, B) (Simões *et al.*, 2022). While these findings suggest that there may be some antagonization of the RQC upon overexpression of Rad6, it is unlikely that such high expression would occur in innate conditions. Additionally, this potential antagonization is not dependent on the ubiquitinating activity of Rad6 nor Rad6's ability to bind to the ribosome, and thus suggests there is no competition for ribosome targets between the RTU and RQC pathways.

RTU and RQC induction are crucial for distinct activation of stressor-specific cellular response

Our characterization of the dynamics of RTU and RQC induction in H_2O_2 and 4-NQO stress suggests that they are induced by specific stress and target different subpopulations of ribosomes. However, the biological significance of RTU-specific induction in H_2O_2 and RQC-specific induction in 4-NQO remains unknown. To determine the contribution of each of the RQC and RTU pathways in regulating translation in oxidative stress, we measured the rate of active translation by HPG incorporation in cells deleted for *HEL2 and RAD6* (Fig 5A). First, we showed that exposure to either H_2O_2 or 4-NQO show decreased translation rate compared to untreated rates in wild-type cells (Fig 5A), with a 10-fold decrease in H_2O_2, a 4-fold decrease in the lower concentration of 4-NQO, and a more than 20-fold decrease in the higher concentration of 4-NQO. In alignment with our previous findings (Meydan *et al.*, 2023), H_2O_2-induced suppression of active translation was dependent only on Rad6 expression (Fig 5A). Under low concentration of 4-NQO (In 1 µg/mL), deletion of RAD6 had no significant effect on translation suppression, corroborating our findings that the RTU is not induced by 4-NOQ. Conversely, deletion of *HEL2* caused the translation rate to drop from a 4-fold decrease in WT to a 10-fold decrease in the lower concentration of 4-NQO. This data suggests that RQC activity mitigates translational repression induced by the lower concentration of 4-NQO. Finally, under high 4-NQO concentration (5 µg/mL), the translation rate was drastically reduced in every strain tested, which indicates that the stress

effect overwhelms cellular capacity to sustain translation. These results reinforce the idea that the RTU and RQC pathways indeed respond differently to different oxidative stressors.

In addition to their roles as translation elongation control pathways, both the RTU and RQC are known to interact with the Integrated Stress Response (ISR) and induce further regulation at the initiation state of translation (Meydan *et al.*, 2023; Yan & Zaher, 2021). In yeast, the ISR pathway blocks translation initiation through phosphorylation of the eIF2α translation factor (P-eIF2α) by Gcn2, which decreases the level of competent ternary complex while simultaneously inducing translation of the Gcn4 transcription factor (Pakos-Zebrucka *et al.*, 2016). Previous work by our lab determined loss of the RTU factor, Rad6 decreases dysregulates eIF2α phosphorylation in peroxide stress (Meydan *et al.*, 2023). Additionally, deletion of the RQC factor HEL2 was reported to further activate eIF2α phosphorylation in steady state and MMS stress (Meydan & Guydosh, 2020; Yan & Zaher, 2021). Thus, we hypothesize that the distinct effects of the RTU and RQC on translation rate in H_2O_2 and 4-NQO stress could be due to differential induction of the ISR. To measure ISR induction, we measured the amount of phosphorylated eIF2α in H_2O_2 and 4-NQO for WT, *rad6Δ*, and *hel2Δ* (Fig 5B). In H_2O_2 stress, P-eIF2α increased in wild-type and *hel2Δ* suggesting Hel2 is not required to activate the ISR. Deletion of *RAD6*, however reduced P-eIF2α compared to WT, suggesting the RTU is important for ISR activation in H_2O_2 stress. Next in 1 µg/mL 4-NQO, we detected P-eIF2α in all strains and at similar levels to those observed for WT in 0.6 mM H_2O_2. Finally, treatment with 5 µg/mL 4-NQO, which leads to increased translation arrest (Fig 5A) induced high levels of P-eIF2α regardless of Rad6 or Hel2 expression. Our results suggest that at low levels of stress, different quality controls pathways can be induced to regulate protein synthesis, while the ISR will display moderate activation. In response to acute stress, ISR becomes the predominant pathway controlling protein synthesis.

Our findings suggest that ISR induction is dependent on the stress intensity. However, it was unclear how effective H_2O_2 and 4-NQO are in inducing global oxidative stress. To better compare stress intensity across stressors, we decided to measure the levels of Tsa2 as a proxy for cellular levels of ROS. Western blot of endogenous myc-tagged Tsa2 was used as a readout for cellular levels of reactive oxygen species (ROS). While Tsa2 protein expression was induced H_2O_2, we observed little effect due to treatment with either concentration of 4-NQO (Fig S5). This finding suggests that 4-NQO activation of the ISR is due to its mRNA damaging capacity than its ability to induce oxidative stress.

To determine if induction of Gcn4 synthesis in either H_2O_2 or 4-NQO occurred in a stress and pathway specific manner, we measured the production of a *GCN4-lacZ* in our main strains (wild-type, *hel2Δ*, and *rad6Δ*) (Fig 5C)(Meydan *et al.*, 2023). Gcn4 expression was significantly increased in the absence of Hel2 in both untreated and 1 µg/mL 4-NQO treated conditions, but not in H_2O_2 stress. There was also no significant difference in *Gcn4-lacZ* in 5 µg/mL 4-NQO, again suggesting this concentration of oxidizing agent surpasses the levels at which cells activate stress response and recovery mechanisms. The increase in *Gcn4-lacZ* expression supports the notion that RQC activity mitigates ISR activation in the low concentration of 4-NQO stress. Finally, our findings corroborate the claim that the RQC pathway is specifically activated in and responsive to 4-NQO and not H_2O_2 stress.

As Gcn4 is known to induce translation of stress-response proteins, we asked whether the targets of Gcn4 were differentially expressed in a stress and pathway-specific manner. To investigate, we mined pre-existing RNA-seq data to quantify differential expression of Gcn4 target

transcripts due to different stress and pathway control. Previous work by the lab identified higher expression of Gcn4-target transcripts in H_2O_2 stress in *rad6Δ* compared to WT cells(Meydan *et al.*, 2023). While we were not able find RNAseq data for cells treated with 4-NQO stress, we utilized RNAseq data from cells treated with MMS stress in *hel2Δ* and WT cells as a proxy for RQC induction through mRNA damage (Yan & Zaher, 2021). Analysis of MMS stress induced transcription of Gcn4 target genes revealed 280 targets of Gcn4 to be differentially expressed in MMS stress compared to untreated cells (Fig 5D). Analysis of these targets in a *HEL2* deleted background showed further upregulation of these Gcn4-targeted transcripts. Analysis of transcript expression change due to H_2O_2 stress, however, revealed statistically significant changes in only 51 genes, and at much lower fold-change than was detected in MMS stress. From this data, it is evident that the mRNA transcripts differentially expressed due to H_2O_2 are distinct from those expressed in response to nucleotide damaging MMS. This suggests that the stress-specific activity of each the RQC and RTU in H_2O_2 and nucleotide-damaging stress by either 4-NQO or MMS is essential for the proper activation of accurate stress response and recovery mechanisms.

DISCUSSION

We previously showed that K63-linked polyubiquitin occurred at a collection of lysine residues across the ribosome surface after exposure to H_2O_2 stress (Back *et al.*, 2019), but whether ub-modification of these sites occurred in response to stress was unknown. Here we developed a method, Rt-PRM, to simultaneously detect and quantify H_2O_2 stress induced changes in ubiquitination across ribosomal sites. Although we identified a high abundance of ub-modified peptides at well-established RQC sites, our method revealed new ub-modified ribosome sites that accumulate under stress independently of the RQC enzyme Hel2 (Fig 2D). Identification of these sites also opens new avenues for research into how this site-specific ubiquitination mediates RTU-related ribosome pausing at the pre-translocation stage of elongation (Zhou *et al.*, 2020), or on XIP sequences (Meydan *et al.*, 2023). Notably, several of these sites are localized to the tRNA exit tunnel and thus serve as ideal candidates for further investigation into the mechanisms underlying translational control. Also of interest, we detected some ubiquitination at known RQC sites in absence of Hel2 (Fig 2C), introducing the possibility that a single ribosome-site can be a target for modification by multiple mechanisms, and opening up new avenues into how the function of these sites changes based on the biological context in which it occurs.

In our proteomics analysis, we identified two H_2O_2-induced ub-modified ribosome sites to be dependent on the E3 ubiquitin ligase, Hel2 (Fig 2C). While previous work has found Hel2-mediated ribosome ubiquitination was induced by 4-NQO oxidative stress (Yan *et al.*, 2019), this is the first finding to show this ub-modification induced by peroxide stress. Through analysis of 4-NQO and H_2O_2-induced ribosome ubiquitination dynamics, we were able to determine that this peroxide-induced Hel2-dependent activity was induced by a different mechanism than that established by 4-NQO stress induction (Fig 3B). As such, further research into the peroxide stress induction of ribosome ubiquitination by Hel2, and its implications for RQC activity must be done to fully dissect the complex mechanisms of stress-induced ubiquitin-mediated translational control. Our analysis did suggest, however, that any peroxide induction of the RQC did not affect the RTU redox burst of K63-linked ubiquitin (Fig 3A), and thus we hypothesized that the RQC targets a distinct population of ribosomes than those modified by the RTU. This hypothesis was

further supported by our findings that the antagonistic relationship between Rad6 expression and RQC clearance of a 6xCGA reporter was not dependent on Rad6's ubiquitinating ability or the strength of its association with ribosomes (Fig 4F, Fig S3 C-D), thus excluding Rad6 ubiquitination of the ribosome as the driver of this interaction. This does, however, warrant further study into how overexpression of Rad6 antagonizes RQC activity in a non-RTU manner.

Our investigation into the contributions of the RTU and RQC to the cellular stressor-specific response revealed two distinct mechanisms of ISR induction. In agreement with our previous findings (Meydan *et al.*, 2023), Rad6 was crucial to facilitate translational repression and induce translation of Gcn4 via a P-eIF2α-independent mechanism in H_2O_2 stress. In this study, we have established that this Rad6-dependent mechanism is not induced in response to 4-NQO stress, indicating that this is specific to peroxide and not all oxidative stress exposures (Fig 5A-C). Alternatively, we found the Hel2 to mitigate translational suppression in the lower concentration of 4-NQO (1 µg/mL), but not in H_2O_2 stress (Fig 5A). The effect of this RQC mitigation was again observed in the induction of Gcn4 as *hel2Δ* showed much higher levels of *Gcn4-lacZ* expression than WT in both untreated and 1 µg/mL 4-NQO (Fig 5C). This suggests that Hel2 antagonizes activation of the ISR. This Hel2 antagonization of the ISR was not observed in the higher concentration of 4-NQO stress, indicating there is a window of stress intensity in which RQC induction enables the cell to maintain active translation. Once the higher range of stress intensity is achieved, however, it appears that induction of the RQC is not enough to avoid exceeding the cellular limits for stress. In all these findings suggest that RTU induction in peroxide stress acts as an early defense mechanism to shut down translation before damage can occur. Alternatively, it appears that induction of the RQC functions in an attempt to mitigate the effects of already existing damage.

The ribosome is a hub translational control and serves as a common target of several ubiquitin-mediated pathways, among which are the Redox-control of translation by ubiquitin (RTU) and Ribosome-associated protein quality control (RQC). This research underscores the critical role of cellular context in dissecting the complex code of ub-modified ribosome sites, both in their induction and in their ultimate impact on translational regulation. We identified and quantified ribosomal site-specific ubiquitination induced by H_2O_2 stress, explored the impact of different oxidative and alkylative stressors on ribosome protein ubiquitination, and established the contributions of stressor-specific induction of the RTU and RQC to global translational regulation and the cellular stress defense response. As such, this work has revealed key distinctions in the stressor-specific functions of the RTU and RQC, but further investigation into the context-specific roles of ribosome site-specific ubiquitination remains essential to fully dissect the ubiquitin-mediated mechanisms of translational control in response to cellular stress.

MATERIALS AND METHODS

Yeast strains, plasmids, and growth conditions

Microbe strains

All *Saccharomyces cerevisiae* strains used in this study are listed in Table S3. Unless otherwise noted, yeast strains were grown in synthetic defined (SD) medium composed of D-Glucose (BD

Difco, #215510), yeast nitrogen base (BD Difco, #291940), and required amino acids at 30°C and 200 rpm agitation.

This study used the *E. coli* strain NEB10-beta (New England Biolabs #C3019H) grown in LB-medium (Sigma-Aldrich #L3022) at 37°C and 200 rpm agitation.

Strain generation

Standard recombination methods were used to delete and tag genes and were confirmed by PCR. Plasmids were constructed using either T4 ligation (New England Biolabs #M0202L) or HiFi DNA Assembly methods (New England Biolabs, #E2621S). All plasmids used in this study are listed in Table S4.

Growth conditions

For all mass spectrometry experiments, SUB280 and SUB280 *hel2Δ* yeast were grown in synthetic defined (SD) medium (BD Difco, #215510, BD Difco, #291940) and drop-out amino acid medium without Leu and Trp (Sigma, #Y0750). Follow up experiments in SUB280 and W303 derivatives were grown in SD complete media by using dropout amino acid supplements without Ura (Sigma, #Y0751) and supplementing back with Uracil (Sigma, #U0750). SUB62 strain derivatives were grown in (SD) medium composed of D-Glucose (BD Difco, #215510), yeast nitrogen base (BD Difco, #291940) and drop-out amino acid medium without Ura (Sigma, #U0750). Unless specified, yeast cells were cultivated at 30°C at 200 rpm agitation to mid-log phase. Unless otherwise stated, yeast cells were treated for 30 minutes with the following stressors/concentrations: freshly diluted H_2O_2 (peroxide) (Sigma, #216763) was added to a concentration of 0.6 mM or 5 mM, 4-nitroquinoline 1-oxide (4-NQO) (Sigma-Aldrich #N8141) was added to a concentration of 1 µg/mL or 5 µg/mL, Methyl methanesulfonate (MMS) (Sigma-Aldrich #129925) was added to a concentration of 0.1% or 0.33% v/v.

Yeast protein extraction and western blots

Yeast protein extraction

Cells were disrupted by glass-bead agitation at 4°C in standard lysis buffer containing 50 mM Tris-acetate pH 7, 100 mM NaCl, 30 mM MgCl2, 20 mM iodoacetamide (IAM), and 1X protease inhibitor cocktail set I (Sigma, #539131). Cells intended for sucrose sedimentation were disrupted in standard lysis buffer with 1X protease inhibitor cocktail replaced by 1x complete mini EDTA-free protease inhibitor cocktail (Roche #04693159001). 1X Phosphatase Inhibitor (Sigma-Aldrich #P5726) was added to the standard lysis buffer for samples probed for phosphorylated proteins by western blot. Extracts were clarified by centrifugation, and protein concentration was determined via Bradford Assay (Bio-Rad, #5000205).

Ribosome sucrose sedimentation

Yeast lysates were sedimented by ultracentrifugation for 120 min at 70,000 rpm (Beckman Optima Max-TL, TLA-110 rotor) at 4°C in a 50% sucrose cushion buffered in 50 mM Tris-acetate, pH 7.0, 150 mM NaCl, and 15 mM MgCl2. Ribosome pellet was resuspended in same lysis buffer and protein concentration was determined via Bradford Assay (Bio-Rad, #5000205) prior to western blot.

Western blot analysis

Proteins were separated by standard 10-15% SDS-PAGE and transferred to PVDF membrane (ThermoFisher, #88518). Immunoblotting was performed using the antibodies in Table S3. Western blots were quantified using ImageJ Software (Schneider *et al*, 2012), and Student's t-test was used to calculate statistically significant differences with a p-value cutoff of 0.05.

Mass spectrometry experiments

Heavy labeled reference peptide synthesis and characterization

Heavy labeled reference peptides (Table S4) for PRM containing isotopically labeled C-terminal Lysine (13C6,15N2) or Arginine(13C6,15N4) residues were synthesized by JPT Peptide Technologies. Heavy labeled reference peptides were reconstituted in 100 mM Ammonium Bicarbonate (ACN) to a final concentration of 100 pmol/uL.

To generate a spectral library, 200 fmol of stable isotope-labeled peptides were analyzed by LC-MS/MS using a Waters M-Class interfaced to a Thermo Fusion Lumos MS/MS. Liquid chromatography utilized a trap-elute configuration and 90 min gradient. MS/MS used data-dependent acquisition with an orbitrap MS2 resolution of 30,000, AGC target of 5E4, max injection time (IT) of 54 ms and stepped normalized collision energy (NCE) of 30 -/+ 5%. Mass spectra were imported to Skyline (MacLean *et al.*, 2010) to build a spectral library using the MS-Amanda search engine.

Yeast ribosomal peptide preparation

SUB280 or SUB280 *hel2Δ* yeast were grown to mid-log phase in SD medium. Half of the sample was collected, while the remaining sample was treated with 0.6 mM H_2O_2 for 30 minutes at 30°C at 200 rpm agitation. Cells were lysed by glass bead disruption agitation at 4°C in lysis buffer containing 50 mM Tris-acetate pH 7, 100 mM NaCl, 30 mM MgCl2, 20 mM iodoacetamide (IAM), and 1x complete mini EDTA-free protease inhibitor cocktail (Roche #04693159001). Cell extracts were clarified by centrifugation and were sedimented by ultracentrifugation for 120 min at 70,000 rpm (Beckman Optima Max-TL, TLA-110 rotor) at 4°C in a 50% sucrose cushion buffered in 50 mM Tris-acetate, pH 7.0, 150 mM NaCl, and 15 mM MgCl2. Ribosome pellets were resuspended in 250 uL digestion buffer (50 mM ACN pH 8, 50 mM NaCl, 8M Urea). Samples were diluted to < 1 M Urea with 50 mM ACN pH8, and protein concentration was determined by Bradford Assay (Bio-Rad, #5000205). 25 mg of resuspended ribosome pellet was digested with trypsin at a [20:1] protein: protease (w/w) ratio for 4 hours at 32°C. Digests were acidified to a final concentration of 1% FA for at least 15 minutes, clarified by centrifugation, and desalted by Sep-Pak C18 Cartridges

(Waters #WAT051910). Samples were dried by lyophilization and resuspended in IAP buffer from PTMScan HS Ubiquitin/SUMO Remnant Motif (K-ε-GG) Kit (Cell Signaling #59322). K-GG containing heavy reference peptides were pooled and diluted into the IAP buffer resuspension fat a final concentration of 1 fmol per peptide. Samples were incubated for 2 hours at 4°C with K-GG antibody beads and eluted with IAP Elution buffer (0.15% TFA) in accordance with the manufacturer's protocol. Samples were again desalted by C18 Stage Tip cleanup prior to sample resuspension and targeted PRM or LC-MS/MS analysis.

Targeted PRM Mass Spectrometry analysis

The samples of K-GG-enriched peptides were reconstituted in 12 uL, and 3 uL of each was analyzed by LC-MS/MS using a Waters M-Class interfaced to a Thermo Exploris 480 MS/MS (n=5). Liquid chromatography utilized a trap-elute configuration and 90 min gradient. MS/MS used parallel reaction monitoring (targeted MS2) with a resolution of 30,000, AGC target of 200%, max IT of 200 ms and NCE of 30. The scheduled inclusion list used 4 min wide windows and a 3 s cycle time.

Label-free proteomics

The samples of K-GG-enriched peptides were analyzed by LC-MS/MS using a Waters M-Class interfaced to a Thermo Exploris 480 MS/MS (n=5). Liquid chromatography utilized a trap-elute configuration and 90 min gradient. MS/MS used data-independent acquisition (DIA) with a 120,000 resolution precursor scan from 375-1600 m/z, AGC target of 300% and max IT of 45 ms. DIA used 30,000 resolution, AGC target of 1000% and max IT of 60 ms a NCE of 30. DIA windows (20 total) spanned 400-1000 m/z with a window width of 30 m/z and window overlap of 1 m/z. Mass spectra were matched to previously built spectral library in Skyline and quantified.

Statistical Analysis

Statistical analysis of peptide fold-change (FC) statistical significance was computed by student's pair t-test, and multiple testing correction was performed with the Benjamini-Hochberg procedure. Pairwise comparisons were considered to be statistically significant if the FC > 1.5 and $p < 0.05$.

Dual luciferase reporter activity

Yeast strains transformed with Rluc-P2A-X-P2A-Fluc plasmids, where X represents a variable sequence, were grown to mid-log phase in SD complete medium. Cells were pelleted and resuspended in SD Methionine depleted (SD -Met) medium to induce plasmid expression for 60 minutes. Cells were then either left untreated or treated with 0.6 mM H_2O_2 or 4-NQO (1 µg/mL, 5 µg/mL) for an additional 30 minutes under agitation. Cells were then pelleted and disrupted by glass bead agitation at 4°C in 1x Passive Lysis Buffer provided in the Dual-Luciferase Reporter Assay System (Promega #E1910). Extracts were clarified by centrifugation, and protein concentration was determined by BCA assay (ThermoFisher #23225). Luminescence activities of Rluc and Fluc were collected for 3 ug of protein combined with respective substrates 10x diluted and were measured in a Spectra Max M3 (Molecular Devices) plate reader.

Translation rate assays

The indicated SUB280-derived yeast strains were grown to mid-log phase in SD complete medium and back diluted to OD_{600} 0.1-0.2 in SD -Met medium. Cells were treated with 50 uM of HPG (L-Homopropargylglycine, Sigma, #900893) at OD_{600} 0.4-0.5. Cells were collected by centrifugation after 15, 30 and 45 min of HPG incubation at 30°C with agitation. For stress treatment, cells were incubated with 0.6 mM H_2O_2, 1 µg/mL 4-NQO, or 5 µg/mL 4-NQO for 15 min prior to HPG incubation for the times listed above. Pelleted cells were fixed overnight in 70% ethanol at 4°C. HPG conjugation with Alexa Fluor 488 was done with the Click-iT HPG Alexa Fluor Protein Synthesis Assay (ThermoFisher #C10428) per the manufacturer's protocol. Alexa Fluor 488 fluorescent signal was measured in the BD FACS Symphony A1 flow cytometer using a 488 nm laser. FlowJo Software (Becton Dickinson) was used for single-cell population gates, histogram plots, and mean calculations.

Gcn4-lacZ reporter assays

GCN4-lacZ expressing yeast cells from the indicated SUB280-derived strains were grown to mid-log phaser and disrupted by glass bead agitation at 4°C in buffer containing 1x PBS, 40 mM KCl, 10 mM $MgCl_2$. Extracts were clarified by centrifugation and protein concentration was quantified by BCA assay (ThermoFisher #23225). 120 ug of protein was combined with substrate containing 15mM ONPG (2-Nitrophenyl-β-D-galactopyranoside, Goldbio, #N27510), 5mM DTT, 1x PBS, 40mM KCl, and 10mM MgCl2, and incubated for 60 min at 30°C. Absorbance was read at 420 nm in a Tecan Sunrise plate reader (Tecan # 30190079).

Gcn4 target mRNA-seq analysis

RNA-seq data from WT and *hel2Δ* cells in the presence and absence of 0.1% MMS treatment (GSE150790) (Yan & Zaher, 2021) and from WT and *rad6Δ* cells in the presence and absence of 0.6 mM H_2O_2 treatment (GSE226082) (Meydan *et al.*, 2023) were analyzed for differential expression of known targets of Gcn4 transcription regulation. Statistically significant differences in transcript expression were calculated in RStudio using a 2-way ANOVA and post hoc comparisons with multiple testing corrections with the Benjamini-Hochberg procedure.

Quantification and statistical analysis

Sample sizes and statistical tests used in this paper are described in the figure legends, and further details are provided in the methods section. All statistical analyses were performed on RStudio. Differences were considered statistically significant at a pvalue <0.05. For multiple comparison analyses, significant changes were calculated by ANOVA contrasts ($p<0.05$) or through multiple testing correction with Benjamini-Hochberg procedure.

REFERENCES

Back S, Gorman AW, Vogel C, Silva GM (2019) Site-Specific K63 Ubiquitinomics Provides Insights into Translation Regulation under Stress. *J Proteome Res* 18: 309-318

Barros GC, Guerrero S, Silva GM (2023) The central role of translation elongation in response to stress. *Biochemical Society Transactions* 51: 959-969

Barros GC, Requião RD, Carneiro RL, Masuda CA, Moreira MH, Rossetto S, Domitrovic T, Palhano FL (2021) Rqc1 and other yeast proteins containing highly positively charged sequences are not targets of the RQC complex. *J Biol Chem* 296: 100586

Chen KY, Park H, Subramaniam AR (2024) Massively parallel identification of sequence motifs triggering ribosome-associated mRNA quality control. *Nucleic Acids Research*

de Nadal E, Ammerer G, Posas F (2011) Controlling gene expression in response to stress. *Nature Reviews Genetics* 12: 833-845

Dougherty SE, Maduka AO, Inada T, Silva GM (2020) Expanding Role of Ubiquitin in Translational Control. *Int J Mol Sci* 21

Erpapazoglou Z, Walker O, Haguenauer-Tsapis R (2014) Versatile roles of k63-linked ubiquitin chains in trafficking. *Cells* 3: 1027-1088

Garshott DM, Sundaramoorthy E, Leonard M, Bennett EJ (2020) Distinct regulatory ribosomal ubiquitylation events are reversible and hierarchically organized. *eLife* 9: e54023

Gasch AP, Spellman PT, Kao CM, Carmel-Harel O, Eisen MB, Storz G, Botstein D, Brown PO (2000) Genomic Expression Programs in the Response of Yeast Cells to Environmental Changes. *Molecular Biology of the Cell* 11: 4241-4257

Higgins R, Gendron JM, Rising L, Mak R, Webb K, Kaiser SE, Zuzow N, Riviere P, Yang B, Fenech E *et al* (2015) The Unfolded Protein Response Triggers Site-Specific Regulatory Ubiquitylation of 40S Ribosomal Proteins. *Mol Cell* 59: 35-49

Holcik M, Sonenberg N (2005) Translational control in stress and apoptosis. *Nature Reviews Molecular Cell Biology* 6: 318-327

Inada T (2020) Quality controls induced by aberrant translation. *Nucleic Acids Research* 48: 1084-1096

Liu P, Gan W, Su S, Hauenstein AV, Fu T-m, Brasher B, Schwerdtfeger C, Liang AC, Xu M, Wei W (2018) K63-linked polyubiquitin chains bind to DNA to facilitate DNA damage repair. *Science Signaling* 11: eaar8133

Llácer Jose L, Hussain T, Marler L, Aitken Colin E, Thakur A, Lorsch Jon R, Hinnebusch Alan G, Ramakrishnan V (2015) Conformational Differences between Open and Closed States of the Eukaryotic Translation Initiation Complex. *Molecular Cell* 59: 399-412

MacLean B, Tomazela DM, Shulman N, Chambers M, Finney GL, Frewen B, Kern R, Tabb DL, Liebler DC, MacCoss MJ (2010) Skyline: an open source document editor for creating and analyzing targeted proteomics experiments. *Bioinformatics* 26: 966-968

Madiraju C, Novack JP, Reed JC, Matsuzawa SI (2022) K63 ubiquitination in immune signaling. *Trends Immunol* 43: 148-162

Manohar S, Jacob S, Wang J, Wiechecki KA, Koh HWL, Simões V, Choi H, Vogel C, Silva GM (2019) Polyubiquitin Chains Linked by Lysine Residue 48 (K48) Selectively Target Oxidized Proteins In Vivo. *Antioxid Redox Signal* 31: 1133-1149

Mascarenhas C, Edwards-Ingram LC, Zeef L, Shenton D, Ashe MP, Grant CM (2008) Gcn4 Is Required for the Response to Peroxide Stress in the Yeast Saccharomyces cerevisiae. *Molecular Biology of the Cell* 19: 2995-3007

Matsuo Y, Ikeuchi K, Saeki Y, Iwasaki S, Schmidt C, Udagawa T, Sato F, Tsuchiya H, Becker T, Tanaka K *et al* (2017) Ubiquitination of stalled ribosome triggers ribosome-associated quality control. *Nature Communications* 8: 159

Matsuo Y, Inada T (2023) Co-Translational Quality Control Induced by Translational Arrest. *Biomolecules* 13: 317

Matsuo Y, Uchihashi T, Inada T (2023) Decoding of the ubiquitin code for clearance of colliding ribosomes by the RQT complex. *Nature Communications* 14: 79

Meng EC, Goddard TD, Pettersen EF, Couch GS, Pearson ZJ, Morris JH, Ferrin TE (2023) UCSF ChimeraX: Tools for structure building and analysis. *Protein Science* 32: e4792

Meydan S, Barros GC, Simões V, Harley L, Cizubu BK, Guydosh NR, Silva GM (2023) The ubiquitin conjugase Rad6 mediates ribosome pausing during oxidative stress. *Cell Reports* 42

Meydan S, Guydosh NR (2020) Disome and Trisome Profiling Reveal Genome-wide Targets of Ribosome Quality Control. *Molecular Cell* 79: 588-602.e586

Ordureau A, Paulo JA, Zhang W, Ahfeldt T, Zhang J, Cohn EF, Hou Z, Heo JM, Rubin LL, Sidhu SS *et al* (2018) Dynamics of PARKIN-Dependent Mitochondrial Ubiquitylation in Induced Neurons and Model Systems Revealed by Digital Snapshot Proteomics. *Mol Cell* 70: 211-227.e218

Pakos-Zebrucka K, Koryga I, Mnich K, Ljujic M, Samali A, Gorman AM (2016) The integrated stress response. *EMBO Rep* 17: 1374-1395

Peterson AC, Russell JD, Bailey DJ, Westphall MS, Coon JJ (2012) Parallel reaction monitoring for high resolution and high mass accuracy quantitative, targeted proteomics. *Mol Cell Proteomics* 11: 1475-1488

Schneider CA, Rasband WS, Eliceiri KW (2012) NIH Image to ImageJ: 25 years of image analysis. *Nature Methods* 9: 671-675

Shenton D, Smirnova JB, Selley JN, Carroll K, Hubbard SJ, Pavitt GD, Ashe MP, Grant CM (2006) Global Translational Responses to Oxidative Stress Impact upon Multiple Levels of Protein Synthesis*. *Journal of Biological Chemistry* 281: 29011-29021

Silva GM, Finley D, Vogel C (2015) K63 polyubiquitination is a new modulator of the oxidative stress response. *Nature Structural & Molecular Biology* 22: 116-123

Simões V, Cizubu BK, Harley L, Zhou Y, Pajak J, Snyder NA, Bouvette J, Borgnia MJ, Arya G, Bartesaghi A, Silva GM (2022) Redox-sensitive E2 Rad6 controls cellular response to oxidative stress via K63-linked ubiquitination of ribosomes. *Cell Reports* 39

Sugiyama T, Li S, Kato M, Ikeuchi K, Ichimura A, Matsuo Y, Inada T (2019) Sequential Ubiquitination of Ribosomal Protein uS3 Triggers the Degradation of Non-functional 18S rRNA. *Cell Reports* 26: 3400-3415.e3407

Taymaz-Nikerel H, Cankorur-Cetinkaya A, Kirdar B (2016) Genome-Wide Transcriptional Response of Saccharomyces cerevisiae to Stress-Induced Perturbations. *Front Bioeng Biotechnol* 4: 17

Wilson DN, Doudna Cate JH (2012) The structure and function of the eukaryotic ribosome. *Cold Spring Harb Perspect Biol* 4

Yan LL, Simms CL, McLoughlin F, Vierstra RD, Zaher HS (2019) Oxidation and alkylation stresses activate ribosome-quality control. *Nature Communications* 10: 5611

Yan LL, Zaher HS (2021) Ribosome quality control antagonizes the activation of the integrated stress response on colliding ribosomes. *Molecular Cell* 81: 614-628.e614

Zhou Y, Kastritis PL, Dougherty SE, Bouvette J, Hsu AL, Burbaum L, Mosalaganti S, Pfeffer S, Hagen WJH, Förster F *et al* (2020) Structural impact of K63 ubiquitin on yeast translocating ribosomes under oxidative stress. *Proceedings of the National Academy of Sciences* 117: 22157-22166

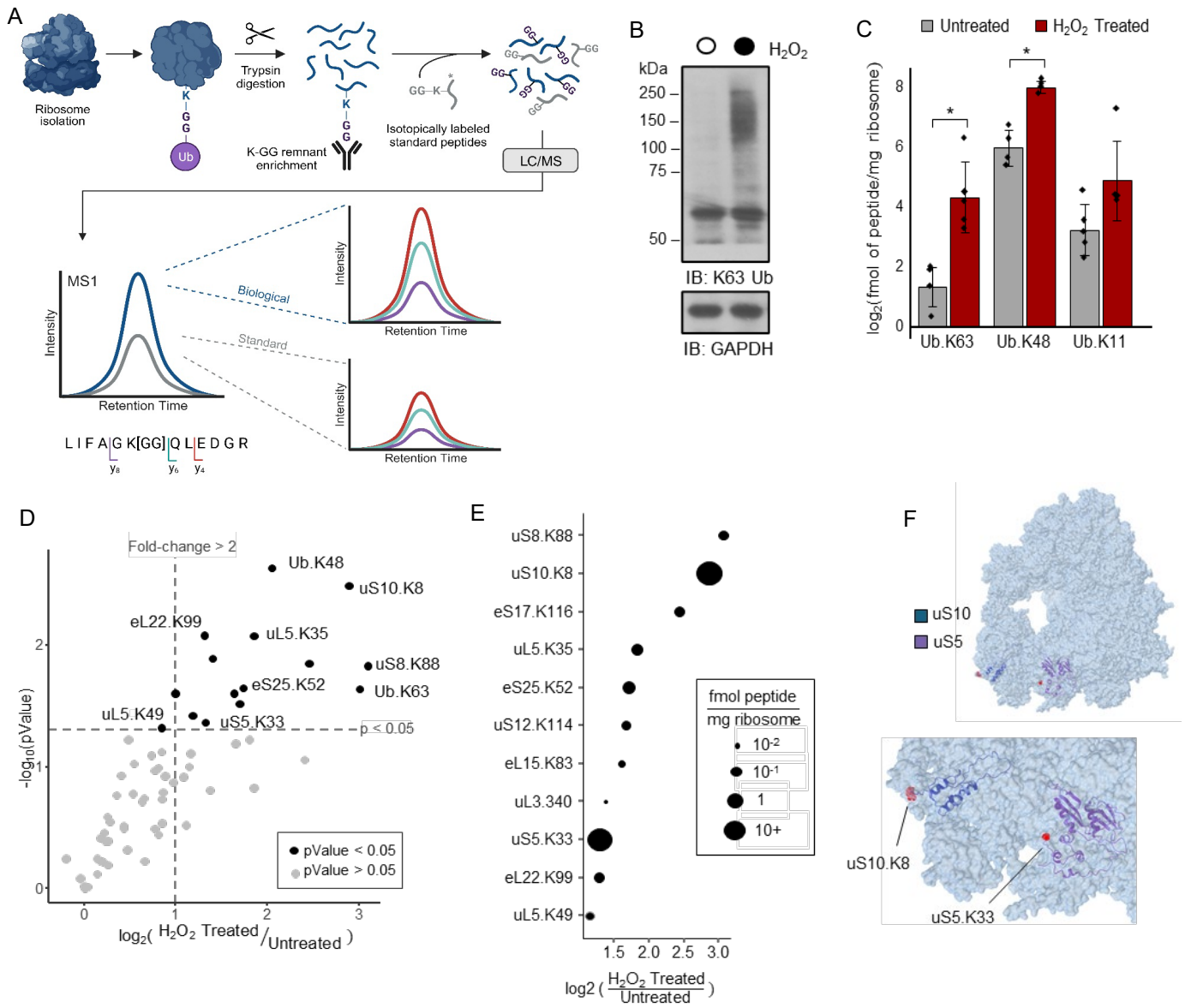

Figure 1

A. Ribosome-target Parallel Reaction Monitoring (Rt-PRM) two-step enrichment for K-GG containing ribosome peptides. Heavy-labeled reference peptides were spiked in before enrichment with K-GG antibody. Peptides were analyzed by LC-MS/MS.

B. Western blot of K63 polyubiquitin chains from cells treated in the presence or absence of 0.6 mM H_2O_2 for 30 minutes. anti-GAPDH was used as a lysate loading control.

C. Cells were treated in the presence or absence of 0.6 mM H_2O_2 and K-GG containing ribosome peptides were isolated and subject to PRM analysis. The abundance (fmol) of K-GG per mg of ribosome for ubiquitin linkage types is shown. Error bars represent SD (n=5). (* pvalue <0.05 by student's paired t-test)

D. Volcano plot of log_2(fold change (FC)) of ub-modified ribosome sites in H_2O_2 Treated and Untreated conditions. p-values calculated by student's paired t-test (n=5).

E. Plot of log2(FC) of K-GG containing ub-modified ribosome sites found to significantly increase from Untreated to H_2O_2 Treated conditions (p<0.05) vs peptide abundance (fmol per mg of ribosome) calculated by normalized to ub-modified ribosome site-specific heavy-peptide.

F. Mapping of most abundant uS10.K8 and uS5.K33 K-GG containing peptides to the 3D ribosome (PDB 6XIR) (Meng et al., 2023; Zhou et al., 2020)

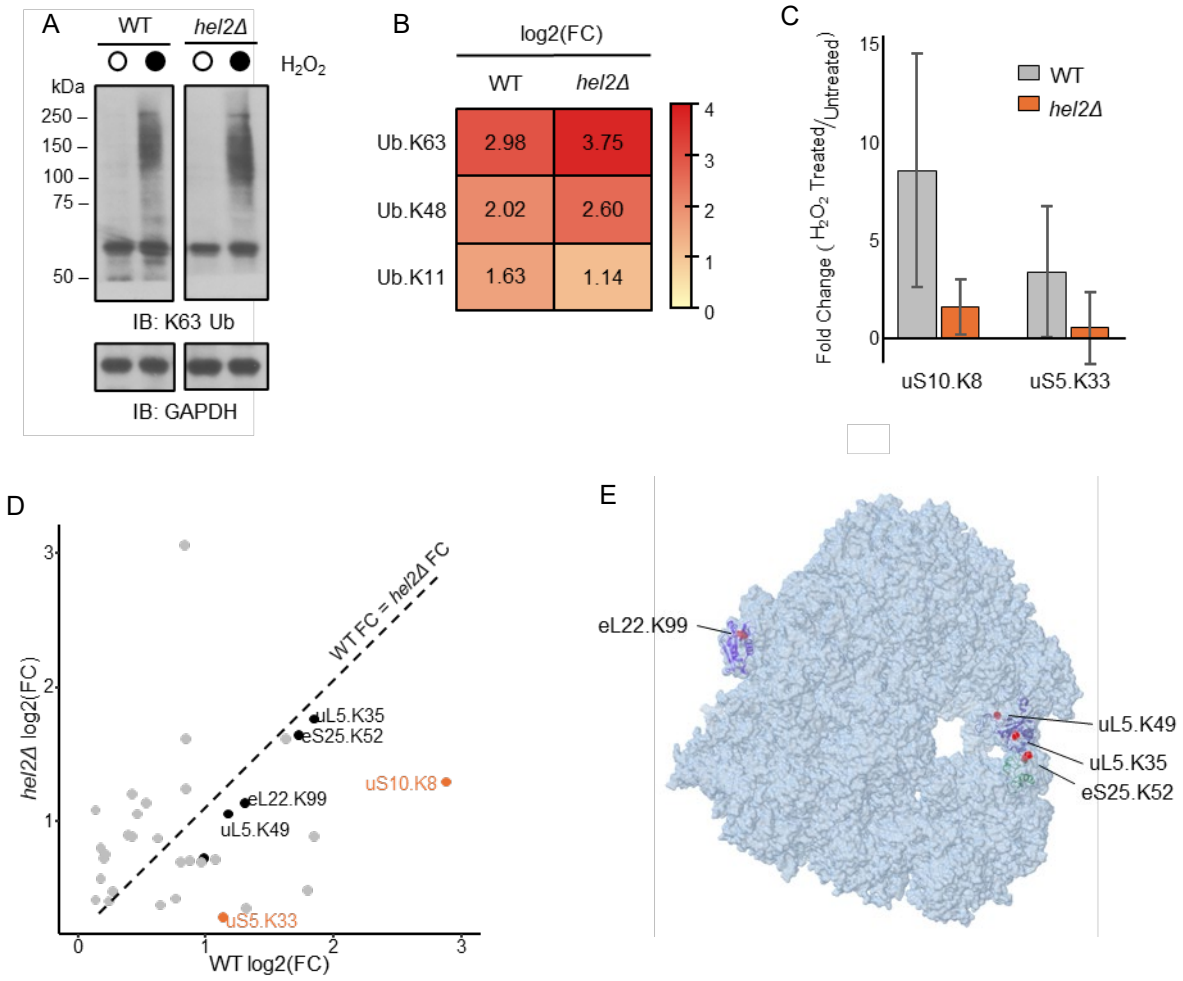

Figure 2.

A. Western blot of K63 polyubiquitin chains from WT and *hel2Δ* cells treated in the presence or absence of 0.6 mM H_2O_2 for 30 minutes. anit-GAPDH was used as a lysate loading control.

B. Heatmap comparing log2(Fold Change (FC)) of ubiquitin linkage peptides quantified before and after H_2O_2 treatment between wild-type (WT) and *hel2Δ* samples.

C. Comparison of the fold change of ubiquitinated uS10.K8 and uS5.K33 peptides in H_2O_2 Treated/Untreated quantified from *hel2Δ* to WT samples

D. Plot of ub-modified ribosome site specific H_2O_2-induced fold change in WT (x-axis) to *hel2Δ* (y-axis). Sites found to undergo statistically significant FC in *hel2Δ* (student's paired t-test, $p < 0.05$) are shown in black.

E. Mapping of Hel2-independent statistically significant H_2O_2-induced ub-modified ribosome sites to the 3D ribosome (PDB 6XIR) (Meng et al., 2023; Zhou et al., 2020).

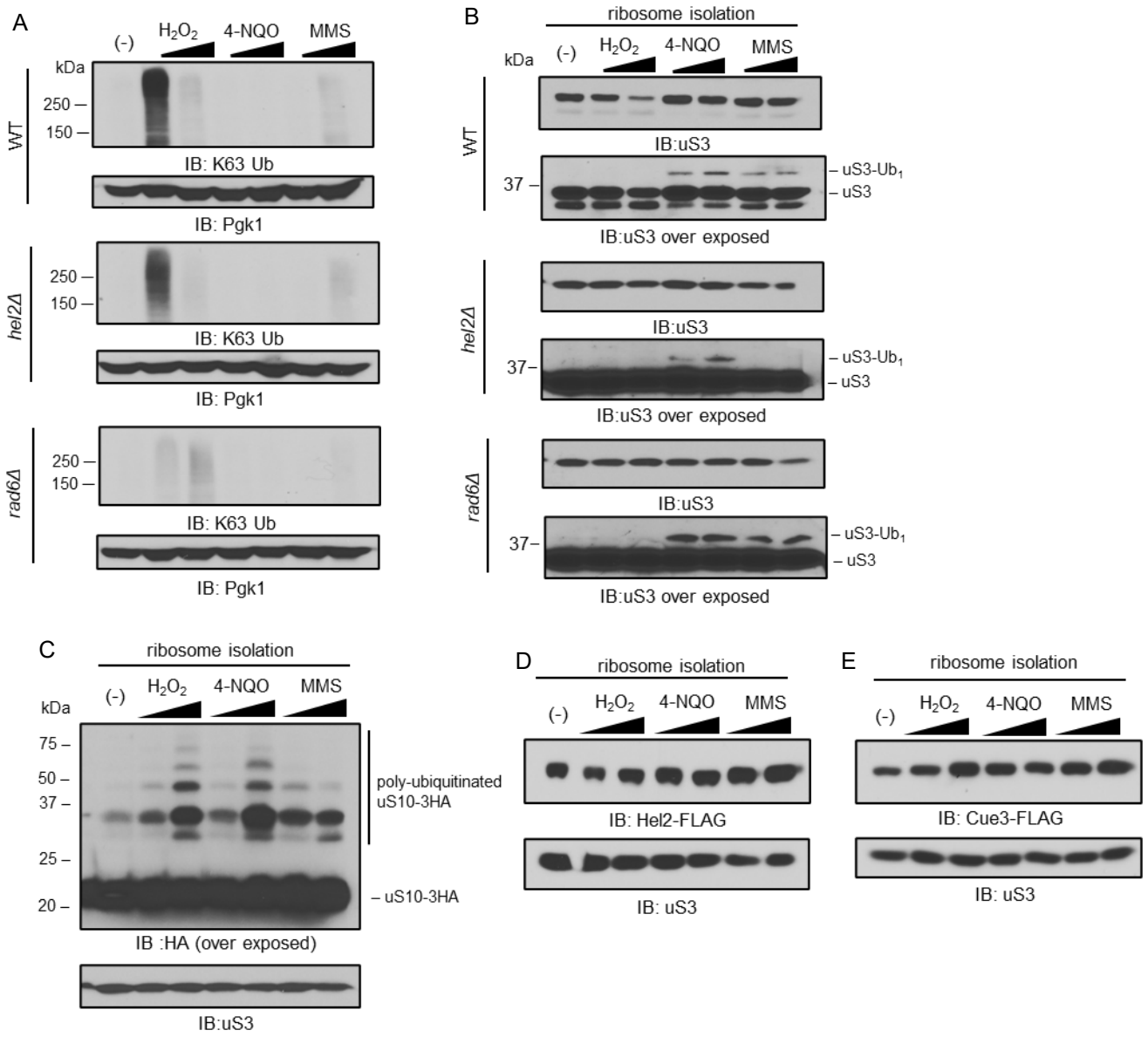

Figure 3.

A. Western blot of K63 polyubiquitination from WT, *hel2Δ*, and *rad6Δ* cells treated with H_2O_2 (0.6 mM, 5mM), 4-NQO (1 µg/mL, 5 µg/mL), and MMS (0.1%, 0.33%). anti-Pgk1 was used as a loading control

B. Western blot of ribosomes isolated from untreated and H_2O_2 (0.6 mM, 5mM), 4-NQO (1 µg/mL, 5 µg/mL), and MMS (0.1%, 0.33%) treated WT, *hel2Δ*, and *rad6Δ* cells probed with anti-uS3

C. Western blot of ribosomes isolated from untreated and H_2O_2 (0.6 mM, 5mM), 4-NQO (1 µg/mL, 5 µg/mL), and MMS (0.1%, 0.33%) treated cells with 3HA tagged uS10 probed with anti-HA. Anti-uS3 was used as a loading control

D. Western blot of K63 polyubiquitination from WT, *hel2Δ*, and *rad6Δ* cells treated with H_2O_2 (0.6 mM, 5mM), 4-NQO (1 µg/mL, 5 µg/mL), and MMS (0.1%, 0.33%). anti-Pgk1 was used as a loading control

E. Western blot of cell lysates and ribosomes isolated from untreated and H_2O_2 (0.6 mM, 5mM), 4-NQO (1 µg/mL, 5 µg/mL), and MMS (0.1%, 0.33%) treated in cells expressing FLAG-tagged Hel2. anti-uS3 was used as a loading control.

F. Western blot of cell lysates and ribosomes isolated from untreated and H_2O_2 (0.6 mM, 5mM), 4-NQO (1 µg/mL, 5 µg/mL), and MMS (0.1%, 0.33%) treated in cells expressing FLAG-tagged Cue3. anti-uS3 was used as a loading control.

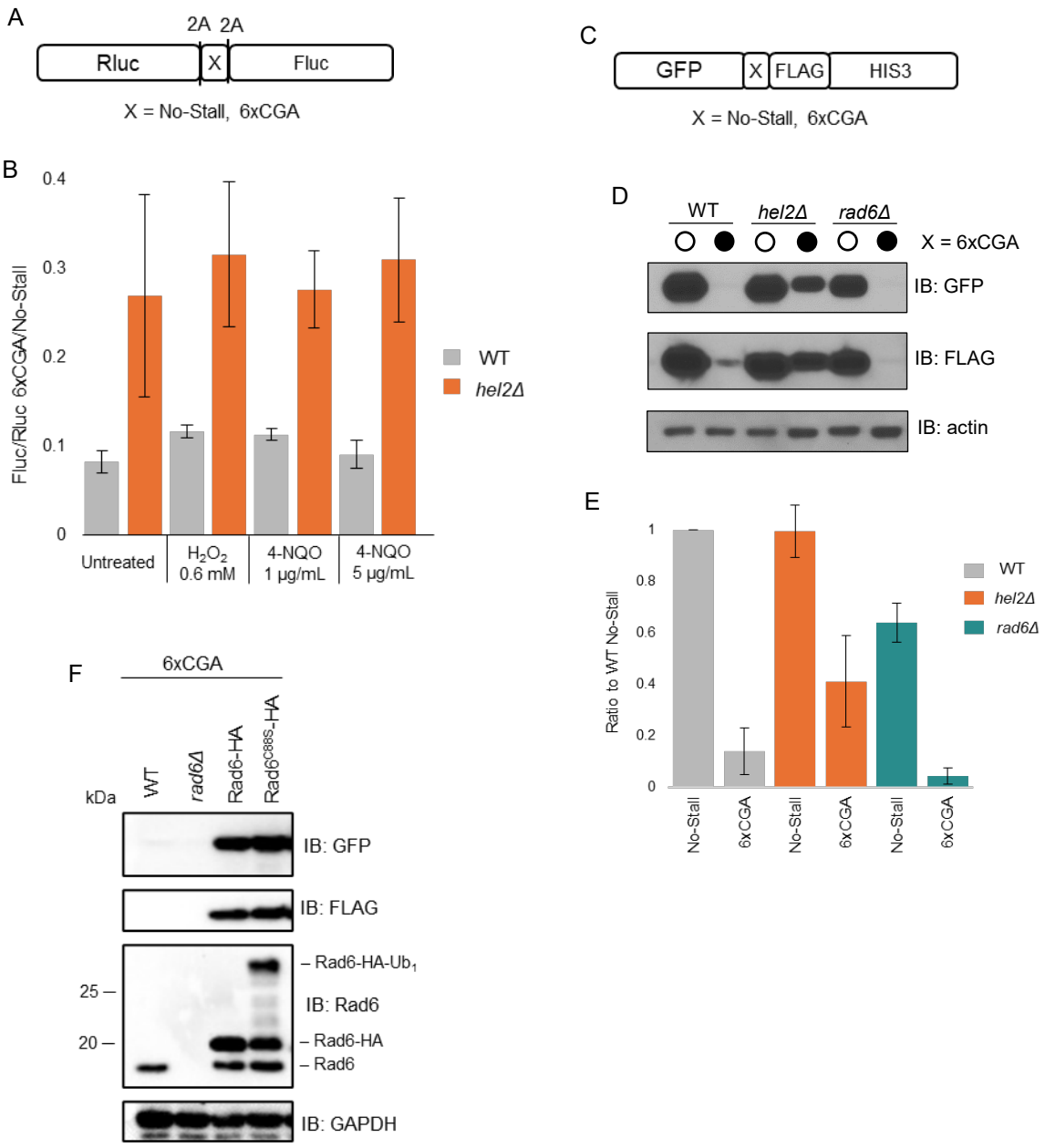

Figure 4.

A. Schematic for the Renilla-Firefly luciferase reporter construct

B. The Ratio of Fluc/Rluc for the 6xCGA reporter compared with a No-Stall reporter in WT and *hel2Δ* in H_2O_2 (0.6 mM) and 4-NQO (1 µg/mL, 5 µg/mL) stress

C. Schematic for the GFP-X-FLAG-HIS3 reporter construct

D. Western blot for full-length GFP-X-FLAG-HIS3 reporter expression for the No-Stall and 6xCGA reporter in WT, *hel2Δ,* and *rad6Δ* with anti-GFP and anti-FLAG. Anti-actin was used as a loading control

E. Quantification of full-length GFP-X-FLAG-HIS3 for the 6xCGA reporter detected with anti-FLAG normalized to No-Stall expression (n=3)

F. Western blot for full-length GFP-X-FLAG-HIS3 reporter expression for the No-Stall and 6xCGA reporter in WT, *rad6Δ,* and *rad6Δ* strains expressing exogenous HA-tagged Rad6, or $Rad6^{C88S}$ with anti-GFP and anti-FLAG. Levels of Rad6 measured by anti-Rad6 and anti-GAPDH was used as a loading control

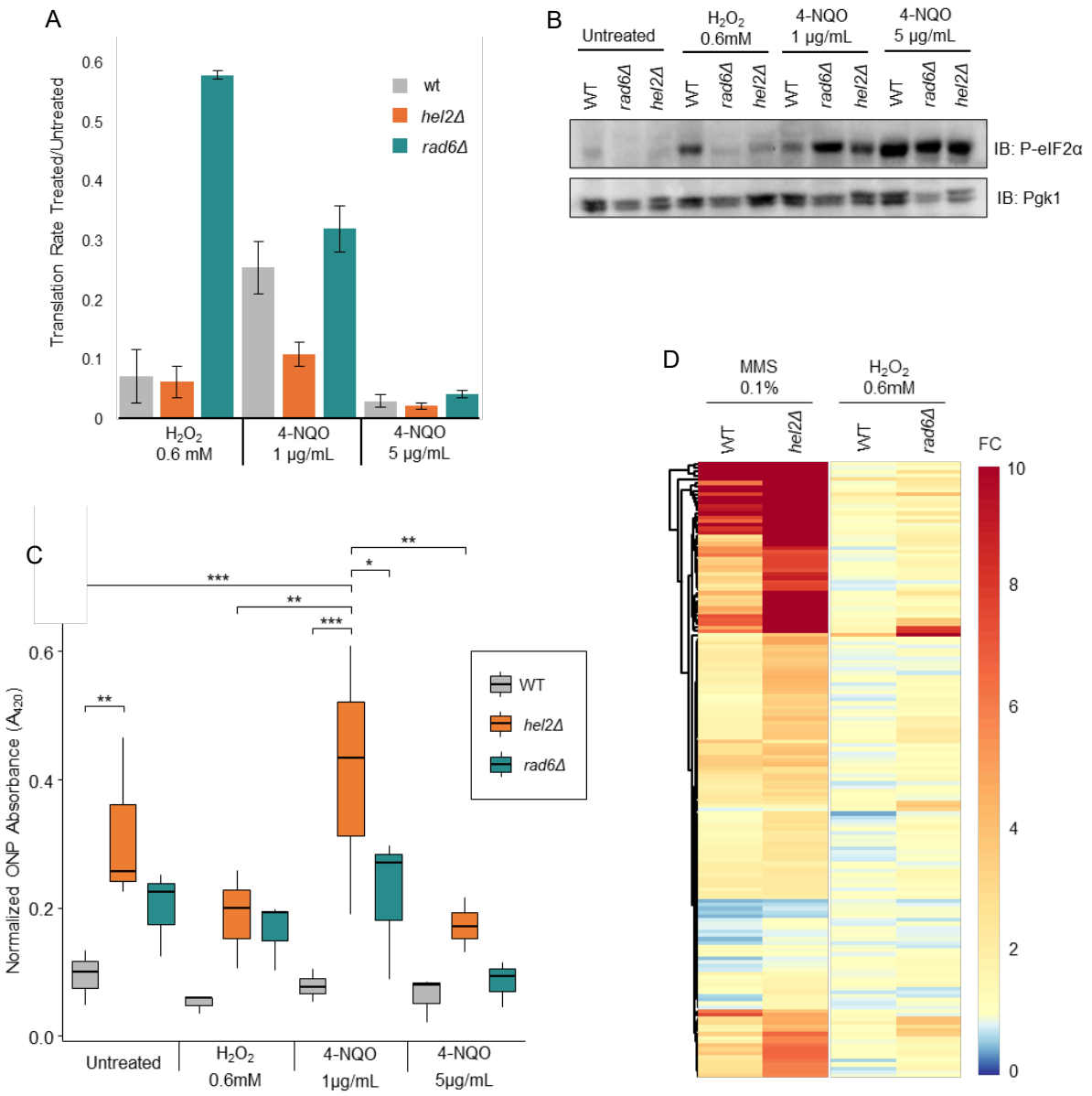

Figure 5

A. Quantification of HPG incorporation during H_2O_2 (0.6 mM) and 4-NQO (1 µg/mL, 5 µg/mL) treatment normalized to untreated in WT, *hel2Δ,* and *rad6Δ*

B. Western blot of phosphorylated eIF2α in untreated and H_2O_2 (0.6 mM) and 4-NQO (1 µg/mL, 5 µg/mL) treated conditions for WT, *hel2Δ,* and *rad6Δ* cells. anti-Pgk1 was used as a loading control.

C. Reporter assay for GCN4 activation by *GCN4-lacZ* fusion construct in WT, *hel2Δ,* and *rad6Δ*. ONPG absorption values detected at 420 nm were normalized to protein levels. Statistical significance was determined by pairwise student's t-test (* = $p < 0.05$, ** = $p < 0.005$, *** = $p < 0.0005$)

D. Heatmap of RNA-seq meta-analysis of known GCN4-targeted stress response transcripts. Datasets from GSE150790 (Yan & Zaher, 2021) and GSE226082 (Meydan et al., 2023) evaluated for differential expression of GCN4 target transcripts due to stress and pathway-specific induction.